Electrophoretic nuclei assembly of MOFs in polyamide membranes for enhanced nanofiltration

Jian Li[a], Riri Liu[b], Junyong Zhu[c,*], Xin Li[d], Shushan Yuan[d], Miaomiao Tian[d], Jing Wang[c], Patricia Luis[e], Bart Van der Bruggen[d], Jiuyang Lin[b,*]

[a] Laboratory of Environmental Biotechnology, School of Environmental and Civil Engineering, Jiangnan University, Wuxi 214122, China

[b] Fujian Provincial Engineering Research Center of Rural Waste Recycling Technology, School of Environment and Resources, Fuzhou University, Fuzhou 350116, China

[c] School of Chemical Engineering and Energy, Zhengzhou University, Zhengzhou 450001, China

[d] Department of Chemical Engineering, KU Leuven, Celestijnenlaan 200F, B-3001 Leuven, Belgium

[e] Materials & Process Engineering (iMMC-IMAP), UCLouvain, B-1348 Louvain-la-Neuve, Belgium

* Corresponding author.

E-mail address: zhujunyong@zzu.edu.cn (J. Zhu); linjiuyang@126.com (J. Lin)

Abstract: Thin film nanocomposite (TFN) polyamide (PA) membranes has drawn increasing attention due to the improved physicochemical properties of the top layer for versatile separation performance. However, the commonly used fabrication approach, lacking a controllable loading of nanofillers, leads to a random and insufficient distribution of nanofillers into the PA layer and generates interfacial defects that deteriorate the membrane performance. Herein, a rational strategy for incorporating metal-organic frameworks (i.e., ZIF-8) into the PA layer via electrophoretic deposition (EPD) was proposed. Driven by an external direct current field, the ZIF-8 nanoparticles were uniformly assembled onto a porous ultrafiltration (UF) substrate for fabrication of high-performance TFN nanofiltration membranes by vacuum-assisted interfacial polymerization (IP). The resultant TFN nanofiltration membrane yielded an enhanced water permeability of 22.4±1.2 $L \cdot m^{-2} \cdot h^{-1} \cdot bar^{-1}$, due to incorporation of ZIF-8 nanoparticles which created extra nano-channels for fast water permeation. Additionally, such an EPD process effectively tailored the membrane surface properties (e.g., zeta potential) and conferred a considerably high rejection for Na_2SO_4 (96.9±0.7%) but a low rejection for NaCl (18.9±2.5%), demonstrating an excellent selectivity between SO_4^{2-} and Cl^- ions. This study highlights the impressive efficacy of the EPD process in precisely anchoring nanomaterials to design high-performance TFN nanofiltration membranes for target separations.

Keywords: ZIF-8 nanoparticles; Electrophoretic deposition; Thin film nanocomposite; Nanofiltration membrane; Enhanced permselectivity

1. Introduction

The scarcity and contamination of freshwater has drawn attention as a global systemic risk [1]. The increasing population with improved living standards and escalating consumption patterns has led to inexorable water demands for agriculture and supplying industries. The 'business as usual' model should be abandoned for a sustainable future as the next generations deserve a high quality of life and wellbeing, but would not carry the environmental cost [2]. Membrane separation technology, especially pressure-driven membranes, has been emerging as a viable alternative to alleviate the enormous challenges of water shortage and contamination due to its high separation efficiency, cost-effectiveness, and environmentally friendliness [3, 4]. Nanofiltration (NF) membranes show an increasing promise to address these challenges. Generally, most of the established commercial NF membranes are thin-film composite (TFC) polyamide-based membranes that are fabricated via interfacial polymerization (IP) [5, 6]. These membranes are capable of removing low-molecular-weight organics (200~1000 Da) and multivalent ions, but the low permeation flux caused by the thick and highly-crosslinked polyamide (PA) layer considerably hampers their cost-effective application in processing large-volume liquid systems [7].

In this regard, thin-film nanocomposite (TFN) membranes are developed by incorporation of nanoparticles in a dense PA layer to create sufficient water transport pathways, thereby allowing for enhanced water permeation [8]. Inspired by this rational design concept, nanoparticles (e.g., zeolite, titanium dioxide, and silicon dioxide) have been extensively applied in preparing TFN membranes to facilitate the water transport

[9-11]. However, the presence of interfacial defects within the PA layer, due to poor affinity of nanoparticles to the polymer matrix and nanoparticle aggregation, inevitably compromises the solute permselectivity of the fabricated TFN membranes.

Porous nanomaterials, e.g., metal-organic frameworks (MOFs), have been explored as functionalized fillers to further intensify the solute permselectivity of TFN membranes [12]. Particularly, MOFs are a typical class of hybrid crystalline materials with an ultrahigh porosity and colossal internal surface areas [13]. The enormous flexibility for organic ligands, metal atoms, and the growth conditions have endowed MOFs with potential applications, e.g., in photoelectric conversion, gas storage, catalysis, and water treatment [14, 15]. It is speculated that MOFs with unique organic linkers have a better affinity with the polymeric matrix than inorganic nanofillers. Therefore, the interfacial defects between MOFs and PA layer are supposed to be significantly reduced, making MOFs to be an ideal candidate in enhancing the filtration performance of the resultant TFN membranes. In addition, MOFs with regular cavities incorporated in the polymer membrane can also serve as an alternative pathway to enhance water permeation. In this context, diverse MOFs, such as ZIF-8, UiO-66, and MIL-101, have been applied to develop advanced TFN membranes [9, 16-18].

However, an inappropriate linkage between nanofiller materials and the PA layer may lead to random distribution and aggregation of nanofillers, potentially resulting in nonselective interfacial defects that can deteriorate the separation performance of TFN membranes. In deposition-based IP, the nanofillers are randomly dispersed in the aqueous or organic phase, followed by the IP reaction to entrap the scattered nanofillers.

Due to a considerably low diffusivity of the nanofillers during the extremely fast IP reaction, only a small fraction of the nanofillers would be successfully intercalated into the PA layer, thus diminishing their functionality in elevating the membrane permeation flux. Therefore, it is of great significance to augment the loading mass and promote an even distribution of the incorporated nanofillers by a rational strategy for enhancing the performance of TFN NF membranes.

Currently, substantial efforts have been made to optimize the loading strategy of the nanofillers before the IP reaction for fabricating novel TFN membranes. For instance, Navarro *et al.* developed an innovative strategy to transfer a monolayer of a Langmuir-Schaefer film of hydrophilic MIL-101 (Cr) for fabrication of TFN membranes [19]. This methodology enables the use of a small quantity of MOFs in making a defect-free PA composite membrane, thereby resulting in an elevated NF performance for organic solvents. Van Goethem *et al.* reported the evaporation-controlled filler positioning method to subtly pre-load ZIF-8 nanoparticles on a porous substrate, followed by IP reaction, to construct TFN NF membranes [20]. The resultant TFN membrane enabled by 0.005 w/v% ZIF-8 nanoparticle exhibited an enhanced permeation flux, compared to the control TFC NF membrane. To overcome the aggregation of the nanofillers in TFN membranes, Wang *et al.* proposed a new layer-by-layer fabrication of PA/ZIF-8 TFN membranes via a two-step synthesis, including *in-situ* growth of a ZIF-8 interlayer and IP reaction [21]. Due to the larger amount of ZIF-8 nanoparticles and the fewer aggregates that are formed, the obtained PA/ZIF-8 TFN membranes evinced an enhanced permeability. Despite the high efficacy of these approaches, the time-

consuming and complicated fabrication steps may impede the progress in developing high-performance TFN NF membranes. Apart from the controlled filler loading approaches, other strategies such as filtration and dip-coating assisted IP techniques are rapidly emerging as promising alternatives to prepare highly permeable PA membranes [22], but the aggregation of nanofillers in the PA layer is still a challenging impediment.

Recently, a strategy of patterned growth of MOFs by electrophoretic deposition (EPD) has raised increasing interest as a potentially feasible alternative [23]. Specifically, an external electric field is utilized to drive the charged nanoparticles, e.g., MOFs, in suspension towards the relevant electrode to form a homogeneous deposition layer without particle aggregation during the EPD process [24, 25]. By controlling the suspension concentration, applied potential, and deposition time during the EPD process, the mass of the deposited nanoparticles and the thickness of the deposition layer can be readily manipulated [23]. In this study, an EPD approach was firstly utilized to evenly immobilize the MOFs nanoparticles (i.e., ZIF-8) into a PA layer for fabrication of advanced MOF-positioned TFN membranes. In this study, the transfer of the ZIF-8 nuclei atop the UF substrate was firstly conducted through tuning the ageing and deposition time. Subsequently, a vacuum-assisted IP reaction was performed using piperazine (PIP) and trimesoyl chloride (TMC) as monomers for NF membrane fabrication. The synthesized TFN membranes were systematically characterized by scanning electron microscopy (SEM), atomic force microscopy (AFM), transmission electron microscopy (TEM) and X-ray photoelectron spectroscopy (XPS). Finally, the effect of ageing and deposition time of the incorporated ZIF-8 nuclei on membrane

separation performance was also studied in details.

2. Materials and methods

2.1 Chemicals and materials

Commercially available polyethersulfone (PES) UF membrane (molecular weight cutoff (MWCO) = 80 kDa) with a pure water permeability of 362.2 $L \cdot m^{-2} \cdot h^{-1} \cdot bar^{-1}$ was purchased from Beijing Separate Equipment Co., Ltd. (China) as support for fabrication of TFN membranes. Zinc nitrate hexahydrate ($Zn(NO_3)_2 \cdot 6H_2O$, 98.0% purity) and 2-methylimidazole (HMIM, 99.0%) obtained from Sigma-Aldrich (Belgium) were applied to synthesize the ZIF-8 nanoparticles. PIP (99.0% purity), TMC (98.0% purity) and n-hexane acquired from Sigma-Aldrich (Belgium) were employed to perform the IP reaction for fabrication of NF membranes. Sodium chloride (NaCl, 99.0% purity), sodium sulfate (Na_2SO_4, 99.0% purity), magnesium chloride ($MgCl_2$, 99.9% purity) and magnesium sulfate ($MgSO_4$, 99.5% purity) purchased from Sigma-Aldrich (Belgium) were applied to test the salt rejection of the resultant NF membranes. Unless otherwise stated, all reagents and solvents were used as received. Deionized water was used throughout the experiments.

2.2 Preparation of TFN membranes

The growth of ZIF-8 nanoparticle on PES membrane substrate with an effective area of 19.6 cm^2 was conducted by an EPD method with a lab-made apparatus at room temperature (**Fig. 1**). The PES substrate mounted on a stainless steel was served as cathode while another bare stainless steel on the other side was used as anode. An aqueous solution (100 mL) containing 0.138 g $Zn(NO_3)_2$ and 2.838 g HMIM was

freshly prepared and homogeneously mixed for synthesis of the ZIF-8 nanoparticles. After a certain period for ageing (i.e., from 0.5 to 2 min) by stirring, the solution was poured between two electrodes. And then, the EPD was performed at a direct current density of 0.72 $mA \cdot cm^{-2}$. The EPD process was applied for a duration ranging from 0.5 to 2 min. The obtained membranes deposited by the ZIF-8 nuclei were completely rinsed to remove the unreacted reagents from the membrane surface through vacuum filtration of deionized water.

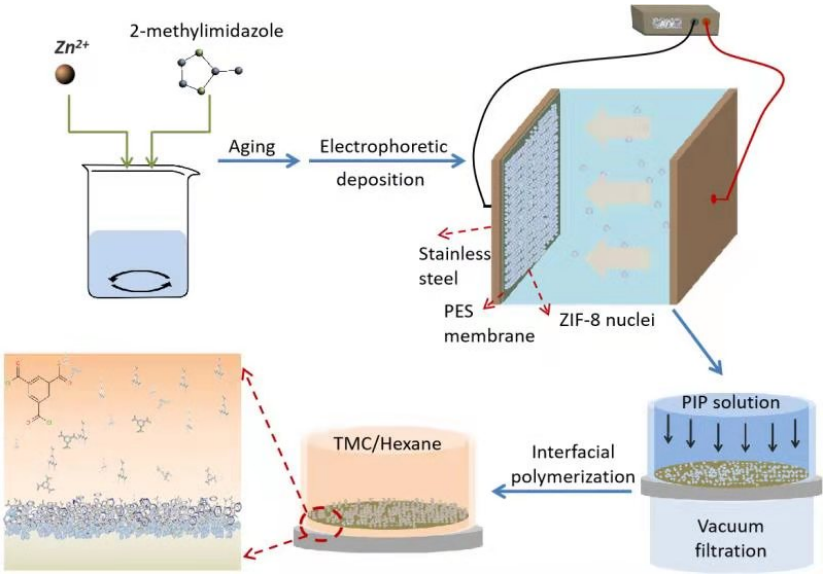

Fig. 1 Fabrication of TFN membranes by constructing ZIF-8 layer via an EPD method and PA layer via a vacuum filtration-assisted IP process

The TFN membranes were constructed through a vacuum filtration-assisted IP method. In detail, an aliquot of the PIP aqueous solution (10 mL, 2 $mg \cdot mL^{-1}$) was filtrated through the UF substrate coated by ZIF-8 nuclei to enable the positioning of PIP in the pore structure of the substrate. The vacuum pump was powered off immediately after the residual liquid was removed by filtration. Afterwards, an aliquot

of the TMC/*n*-hexane solution (10 mL, 1.5 $mg \cdot mL^{-1}$) was poured on the substrate surface to conduct the IP reaction for 1 min. After the organic liquid was removed, the resultant TFN membranes were placed in an oven at 60 ℃ for 3 min. All the synthesized TFN membranes were rinsed and stored in deionized water before use. The parameters for functionalization of membranes and their corresponding labels used in this work are summarized in **Table 1**.

Table 1 Surface functionalization parameters corresponding to the assigned membranes

Membrane	Ageing time (min)	EPD time (min)	IP time (min)
PES	-	-	-
ZIF-8@PES	2	2	/
TFC	-	-	1
TFN-0.5/2	0.5	2	1
TFN-1/2	1	2	1
TFN-1.5/2	1.5	2	1
TFN-2/2	2	2	1
TFN-2/0.5	2	0.5	1
TFN-2/1	2	1	1
TFN-2/1.5	2	1.5	1

2.3 Membrane characterization

The surface morphology of the fabricated TFN membranes was visualized by

scanning electron microscopy (SEM, XL30 FEG, The Netherlands). Specifically, the dried TFN membranes were sputter-coated with platinum and their SEM images were taken at an accelerating voltage of 10 kV. The surface roughness of the membranes was investigated by atomic force microscopy (AFM, Bruker, USA). Root mean squared roughness (R_{rms}) was recorded to identify the change of membrane surface roughness. The nanostructure of the PA layer was inspected by transmission electron microscopy (TEM, JEOL 1230) at an accelerating voltage of 80 kV using Gatan CCD cameras.

The measurement of Fourier transform infrared (FTIR) spectra were conducted to analyze the functional groups of the fabricated membranes by a Nicolet 6700 FTIR spectrometer at the range of 500-4000 cm^{-1}. The elemental composition of membrane surfaces was quantified by an X-ray photoelectron spectroscopy (XPS, Kratos AXIS Ultra DLD, Japan), where an AlKα (1486.6 eV) monochro-matic X-ray source was applied at 200 W. The electron emission angle was fixed at 45° with a sampling depth of 10 nm.

The surface charge of the membranes was measured by an electrokinetic analyzer (Surpass 3, Anton Paar GmbH, Austria). Specifically, a 1.0 mM KCl solution was used as electrolyte solution at pH = 6.0 ±0.2 during zeta potential measurement. The water contact angle of the membranes was performed by the optical surface analyzer (DSA 10 Mk2, KRüSS GmbH Germany) at room temperature with 5 μL DI water and the final value was calculated based on an average of five randomly selected locations. Fourier transform infrared (FTIR) spectra of the membranes were obtained on a Nicolet 6700 FTIR spectrometer in the range of 500-4000 cm^{-1}. The MWCO of the obtained

membranes were determined by the separation of a 200 mg/L polyethylene glycol (PEG, molecular weight of 200, 300, 400 and 600 Da) solutions.

2.4 Water permeability and salt rejection

Water permeability and salt rejection were determined to evaluate the membrane permeation performance by employing a dead-end cell (HP4750 stirred cell, Sterlitech Crop., USA). A membrane coupon with an effective surface area of 14.6 cm^2 (diameter of 4.31 cm) was pre-pressurized until a steady water permeation was achieved. The filtration of 250 mL salt solutions (NaCl, $MgCl_2$, Na_2SO_4, and $MgSO_4$) with a concentration of 1.0 $g \cdot L^{-1}$ was conducted separately to investigate the separation performance of the fabricated TFN membranes at room temperature and 4 bar. The membrane permeability (J) and salt rejection (R) were calculated based on the following equations:

$$J = \frac{V}{A \times \Delta t \times P} \quad (1)$$

$$R = \left(1 - \frac{C_P}{C_f}\right) \times 100\% \quad (2)$$

where A is the effective surface area of the tested membranes, P is the operation pressure, Δt is the time for permeation, and V is the volume of the permeate. C_f and C_p are the salt concentration of the feed and permeate, respectively.

3. Results and discussion

3.1 Membrane surface morphologies

An even and sufficient distribution of the ZIF-8 nanoparticles onto the PES UF support before IP reaction is crucial as it can potentially facilitate the effective formation of extra nano-channels within the PA layer for enhancing the membrane

performance. **Fig. 2** displays the surface morphology of the PES UF substrate before and after deposition of the ZIF-8 nanoparticles by EPD.

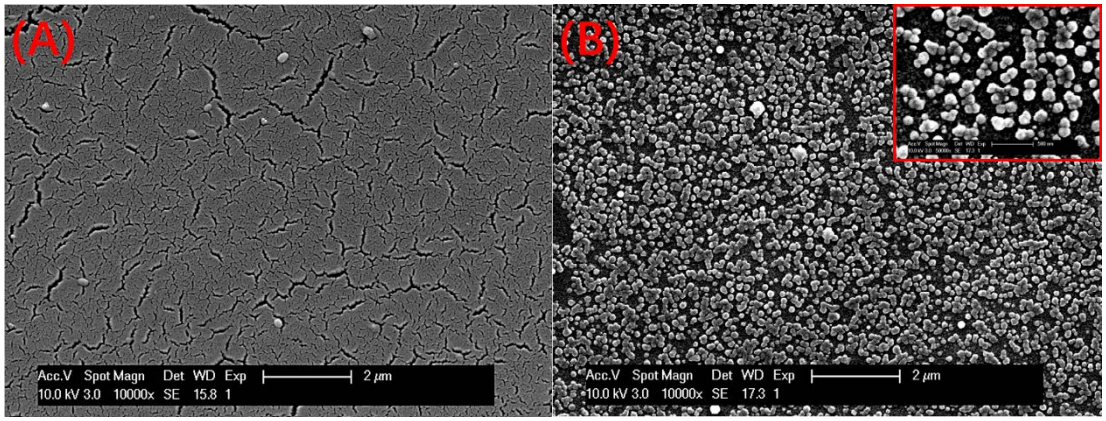

Fig. 2 SEM images of the PES UF support. (A) Pristine; (B) deposited by ZIF-8 via EPD

As evinced in **Fig. 2A**, the PES support shows a uniform and smooth surface. In contrast, a large number of particle-like spots with size ranging ca. 75 nm was observed on the PES support after the EPD process (**Fig. 2B**), indicating the sufficient and even coverage of ZIF-8 nanoparticles on the PES substrate surface without the aggregation of ZIF-8 nanoparticles. This also strongly demonstrates the excellent efficacy of the EPD process for nanoparticle deposition within a very short time (i.e., within 2 minutes). Fig. 3 shows the effect of the ageing time of the incorporated ZIF-8 nuclei on the surface morphology of the fabricated NF membranes. Specifically, the TFC membrane without the loading of the ZIF-8 nanoparticles exhibits an irregular nodule structure on the surface (**Fig. 3A**), due to the diffusion-driven instability caused by vacuum-assisted IP [26]. However, the TFC membrane still shows a considerably smooth surface with a roughness of 2.71±0.14 nm (**Fig. 4A**). This is consistent with the surface characteristics of the poly(piperazine)amide layer [27]. As indicated in **Fig. 3B-3E**, the presence of the

ZIF-8 nuclei in the PA layer plays a significant role in the morphology of the fabricated TFN membranes [21, 28]. The nodular structures originating from the control PA layer started to disappear, whereas some particle-like spots were observed on the surface of these TFN membranes, which would result in an increase of the surface roughness (**Fig. 4B-4E**) [29]. In addition, increasing ageing time from 0.5 to 2.0 min not only distinctly enhanced the loading content of ZIF-8 nanoparticles, but also expanded the size of the ZIF-8 nanoparticles. This result conforms to the growth of the ZIF-8 nuclei with increasing ageing times.

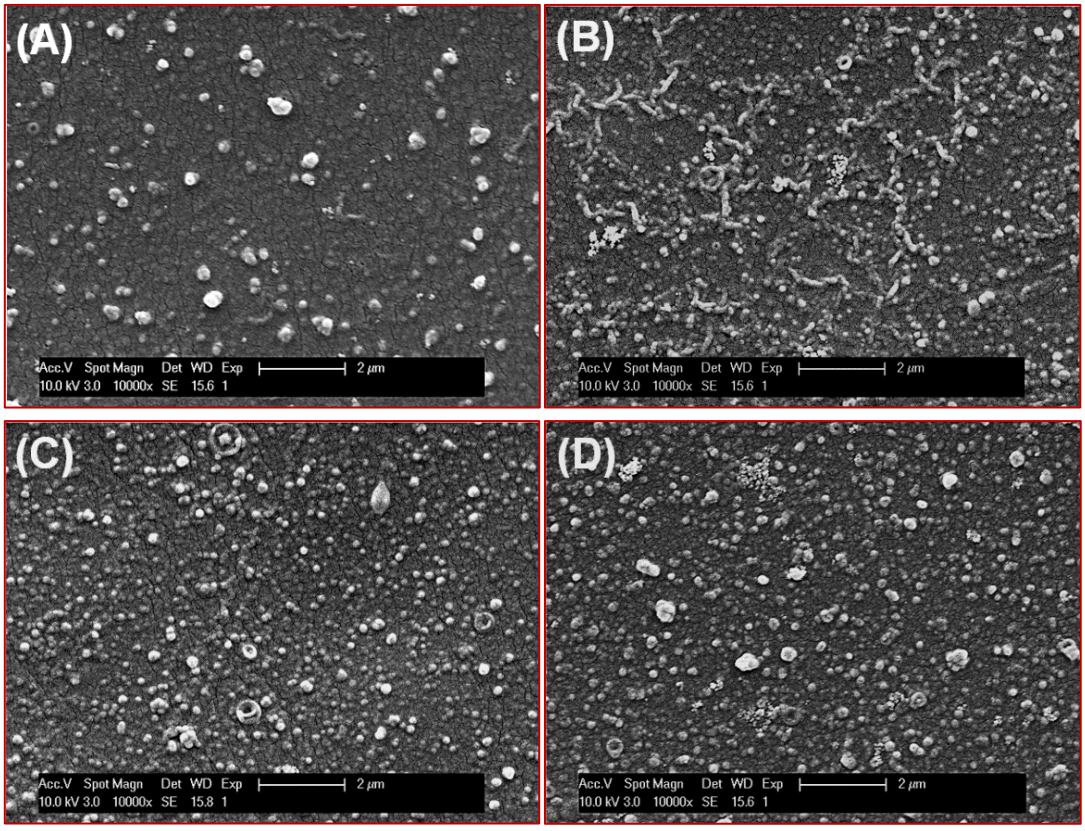

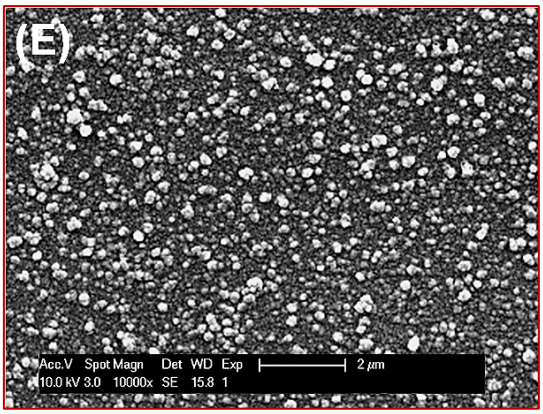

Fig. 3 SEM images of the fabricated NF membranes loaded with the ZIF-8 nanoparticle at different ageing times. (A) TFC; (B) TFN-0.5/2; (C) TFN-1/2; (D) TFN-1.5/2; (E) TFN-2/2

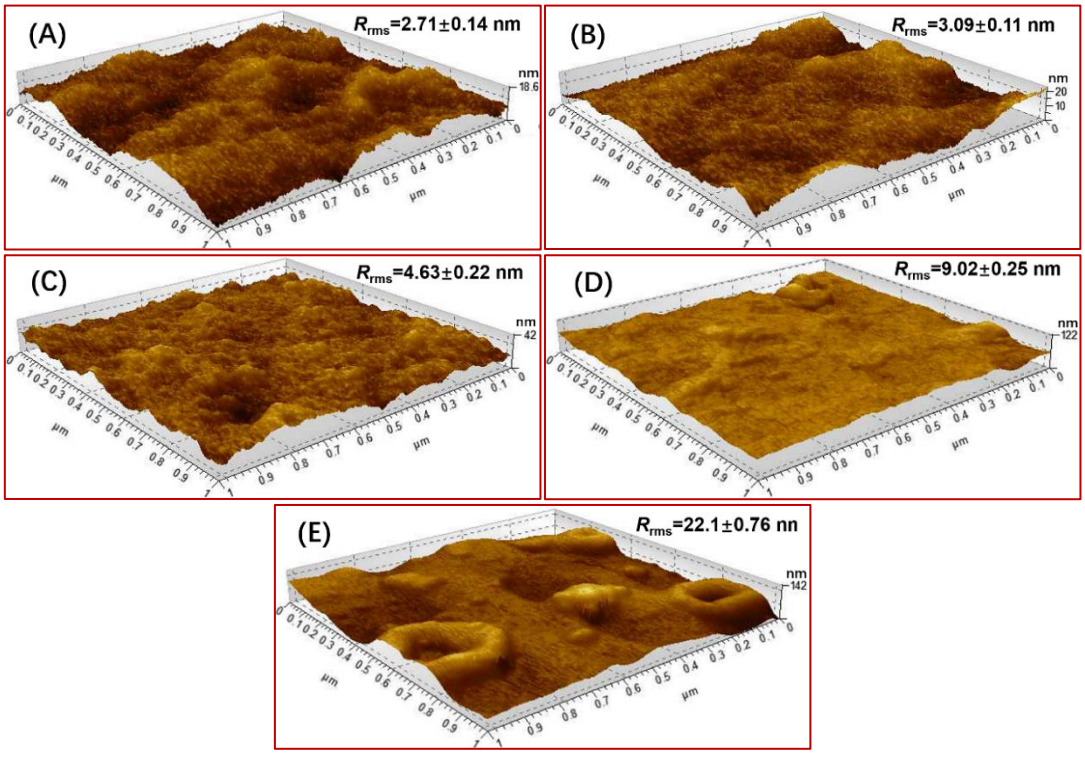

Fig. 4 3D AFM images of the fabricated NF membranes loaded with the ZIF-8 nanoparticles at different ageing times. (A) TFC; (B) TFN-0.5/2; (C) TFN-1/2; (D) TFN-1.5/2; (E) TFN-2/2

Fig. 5 shows the effect of the EPD duration on the surface morphology of the fabricated TFN membranes. With the extension of the EPD time, more ZIF-8 nanoparticles were deposited into the TFN membranes, as evidenced by the particle-like spots in SEM measurement [30]. Specifically, the ZIF-8 nanoparticles were sufficiently and uniformly incorporated into the poly(piperazine)amide layer after a 2-min EPD process. Such a morphology not only elevates the surface roughness of the TFN membranes (**Fig. 6**) for increasing effective permeable area, but also potentially creates more pathways based on the nano-channels of ZIF-8 nanoparticles with increasing loading for promoting the water permeation [31]. The increasing loading of the ZIF-8 nanoparticles into the TFN membranes reconfirms the outstanding efficacy of the EPD process in tailoring the surface morphology of the TFN membranes.

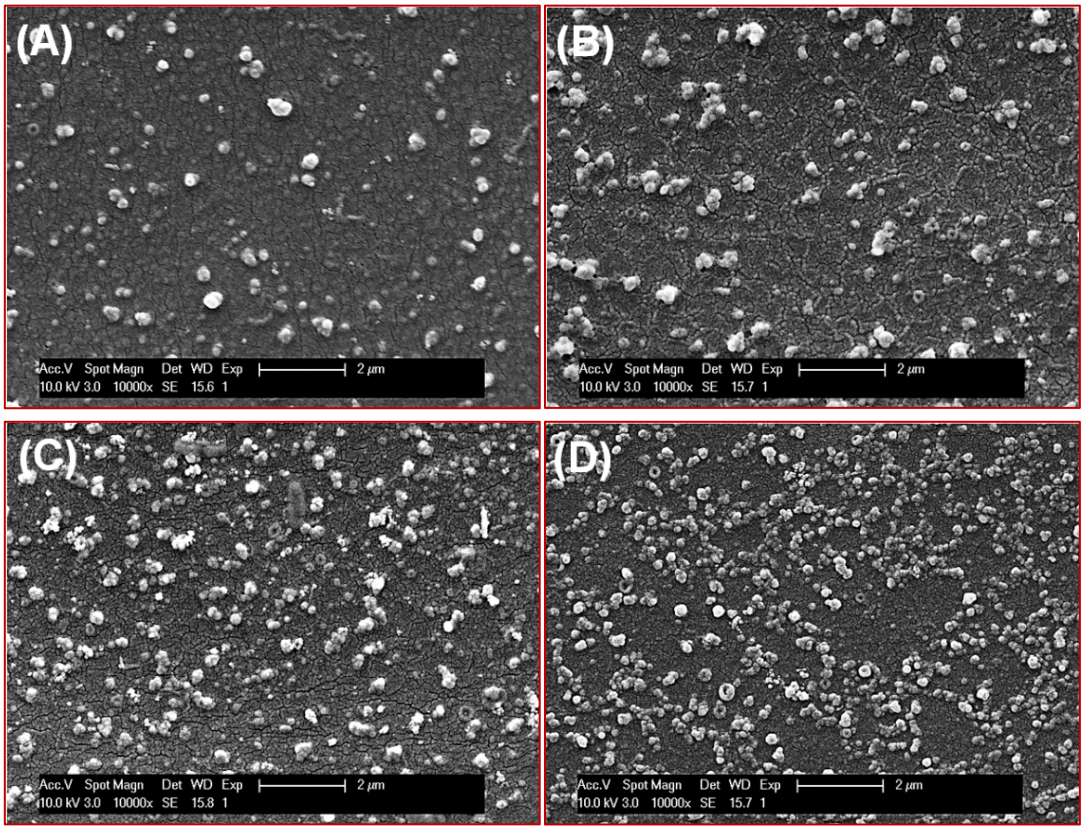

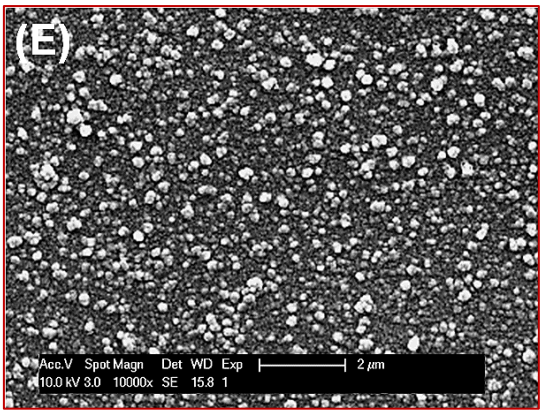

Fig. 5 SEM images of the fabricated NF membranes loaded with the ZIF-8 nanoparticles at variable EPD times. (A) TFC; (B) TFN-2/0.5; (C) TFN-2/1; (D) TFN-2/1.5; (E) TFN-2/2

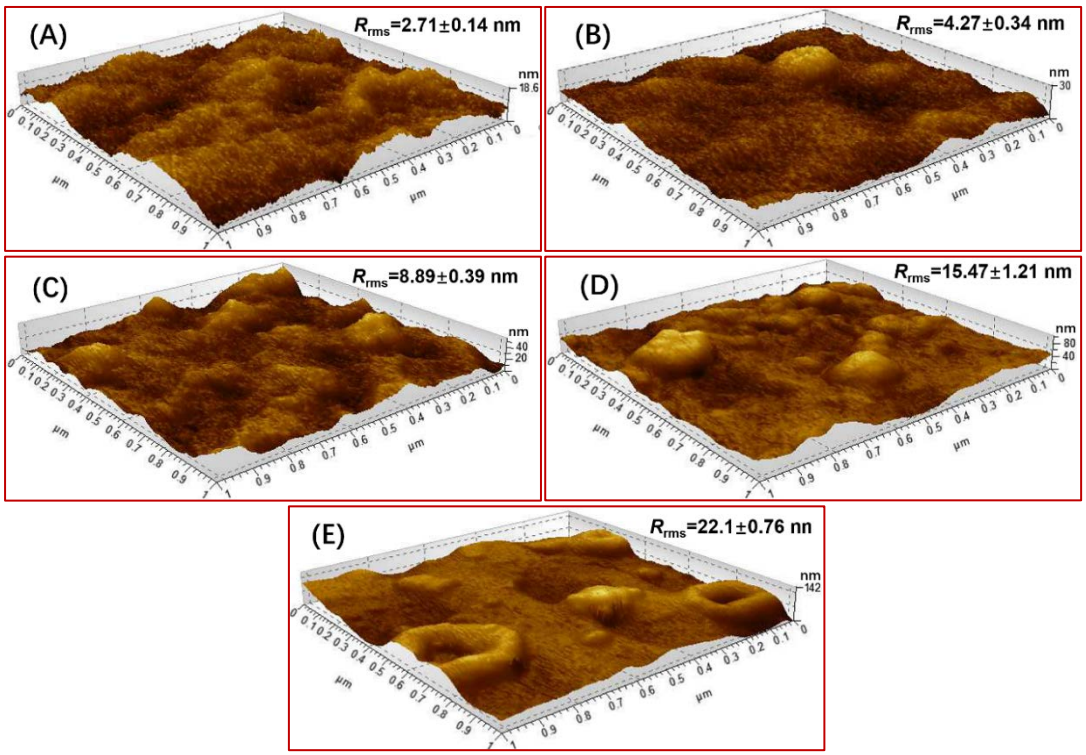

Fig. 6 3D AFM images of the fabricated NF membranes loaded with the ZIF-8 nanoparticles at variable EPD times. (A) TFC; (B) TFN-2/0.5; (C) TFN-2/1; (D) TFN-2/1.5; (E) TFN-2/2

To further investigate the formation process of the TFN membranes loaded with the ZIF-8 nanoparticles via the EPD process, the cross-section of the TFN membrane surface was analyzed by TEM (**Fig. 7**). The thickness of the established dense PA top layer is around 130 nm, which is a typical thickness of a functional layer on a TFC NF membrane [32, 33]. Specifically, a dark and continuous region was observed on TEM images of the PES substrate membrane after modification. For ZIF-8 nanoparticles, a higher mass-contrast led to a darker appearance while the PA layer and PES substrate were much lighter. However, no obvious boundary between the dark and light area was found, suggesting that the ZIF-8 nanoparticles were well anchored onto the PA layer. The sufficient and uniform layout of the ZIF-8 nanoparticles into the membrane surface contributes to the regular nanoporous structure of the TFN membranes, which can potentially enhance the membrane permeability. Apart from the *in-situ* generated ZIF-8 nanoparticles, the abundance of organic ligand within them can also confer a benign compatibility between the ZIF-8 nanoparticles and PA layer [34]. Thus, a consistently stable functional layer was constructed on the TFN membranes.

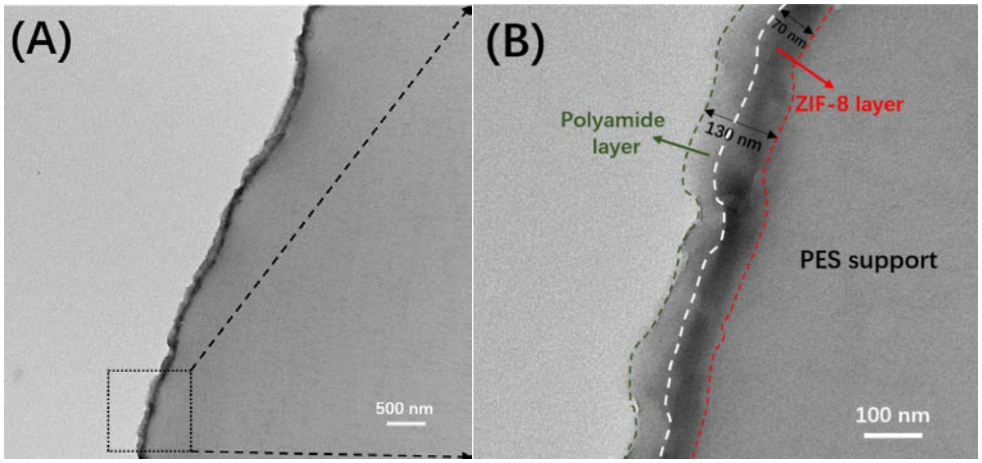

Fig. 7 TEM images of the TFN-2/2 NF membrane after the loading of the ZIF-8 nanoparticles through EDP

3.2 Chemical composition

The FTIR and XPS analysis were further conducted to verify the surface elemental composition of the fabricated TFN membranes (**Fig. 8**).

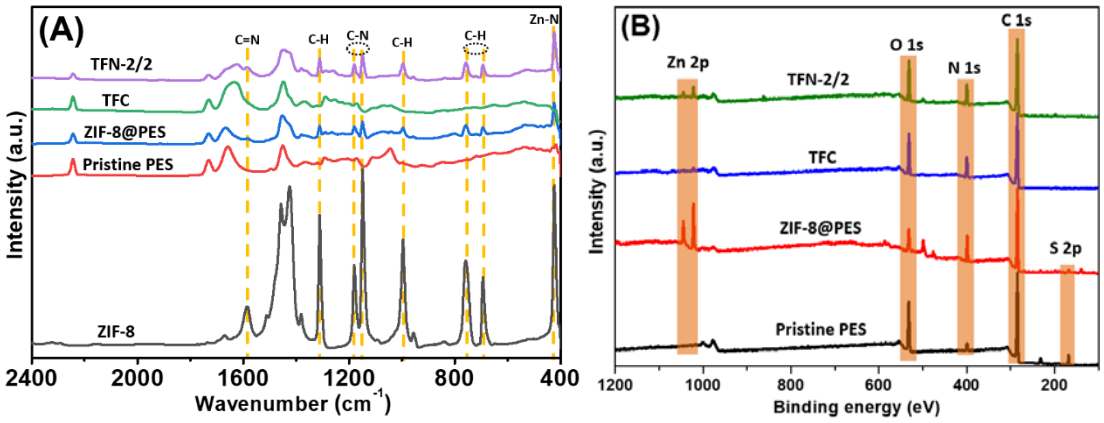

Fig. 8 FTIR (A) and XPS (B) analysis of pristine PES substrate, ZIF-8@PES, TFC, and TFN-2/2 membrane

As shown in **Fig. 8A**, the ZIF-8@PES substrate has extra absorption bands at 1583 cm^{-1}, 1311 cm^{-1}, 1180 cm^{-1}, 1148 cm^{-1}, 758 cm^{-1}, 694 cm^{-1} and 423 cm^{-1}, compared to the pristine PES substrate. Specifically, the absorption band at 423 cm^{-1} and 1583 cm^{-1} corresponded to the Zn-N stretch, respectively [35]. The absorption bands at 1180 cm^{-1} and 1148 cm^{-1} were assigned to the stretching vibration of the C-N group [35]. Meanwhile, the absorption bands at 1311 cm^{-1}, 995 cm^{-1}, 758 cm^{-1} and 694 cm^{-1} were mainly associated to the stretching vibration of the C-H group from imidazole [36-38]. These absorption bands, which were identical with the fabricated ZIF-8 nanoparticles, suggested that the pristine PES substrate was sufficiently covered by the ZIF-8 nuclei. Furthermore, the XPS measurement shows that the pristine PES substrate has the typically intrinsic peaks of C 1s, O 1s, and S 2p at the binding energy of 284.5, 531.6,

and 167.2 eV, respectively (**Fig. 8B**). After the deposition of the ZIF-8 nanoparticles by the EPD process, two extra intensities at the peaks of 1021.2 and 1044.8 eV were detected in the ZIF-8@PES substrate, which are assigned to Zn 2p. Furthermore, a lower intensity of the peak of S 2p was observed as well. In particular, the atomic percentage of Zn element in the ZIF-8@PES membrane deposited by the ZIF-8 nanoparticles increased to 4.52% (**Table 2**), while the atomic percentage of S element was reduced from 4.35% to 1.71%. Therefore, the XPS analysis further confirmed the presence of the ZIF-8 nanoparticles onto the pristine PES substrate. In addition, the TFN-2/2 membrane also has extra absorption bands at 1583 cm^{-1}, 1311 cm^{-1}, 1180 cm^{-1}, 1148 cm^{-1}, 758 cm^{-1}, 694 cm^{-1} and 423 cm^{-1}, compared to the TFC membrane without the loading of the ZIF-8 nanoparticles. This strongly demonstrates the presence of the ZIF-8 nanoparticle in the TFN membranes which were fabricated through IP reaction using the ZIF-8@PES substrate, which is consistent with the SEM observation in **Fig. 3** and **Fig. 5**.

On the other hand, after the IP reaction, the PA layer was strongly attached onto the PES substrate, which resulted in the disappearance of the S 2p peak for the TFC membrane. Similarly, a reduced intensity in the peak of Zn 2p was also observed for the TFN-2/2 membrane incorporated with the ZIF-8 nanoparticles. As reflected by the reduced atomic percentage of Zn element in the TFN-2/2 membrane (**Table 2**), the PA layer was well interconnected with the ZIF-8 nanoparticle layer.

Table 2 Atomic percentage of different elements for membrane surface

Membrane type	Element composition (wt.%)				
	C	N	O	S	Zn
PES substrate	73.67	2.95	19.03	4.35	-
ZIF-8@PES	72.67	12.36	8.74	1.71	4.52
TFN-2/2	73.94	10.72	13.98	0.41	0.95

3.3 Filtration performance

Various salts (i.e., NaCl, $MgCl_2$, Na_2SO_4, and $MgSO_4$) were applied to evaluate the filtration performance of the resultant TFN NF membranes (**Fig. 9**). The PES substrate with a high MWCO (80 kDa) showed a free salt passage. After IP without the incorporation of the ZIF-8 nanoparticles, the TFC NF membrane possessed a dense and compact surface structure (MWCO of 382 Da, see **Supplementary Fig. S1**), enabling a Na_2SO_4 rejection of 98.4±0.2% with a reduced pure water permeability of 9.9±0.5 $L \cdot m^{-2} \cdot h^{-1} \cdot bar^{-1}$. The dense surface structure of the TFC NF membrane with highly negative charges led to a higher resistance to ions due to the synergistic effect of size exclusion and electrostatic repulsion, thus hindering the permeation of Na_2SO_4.

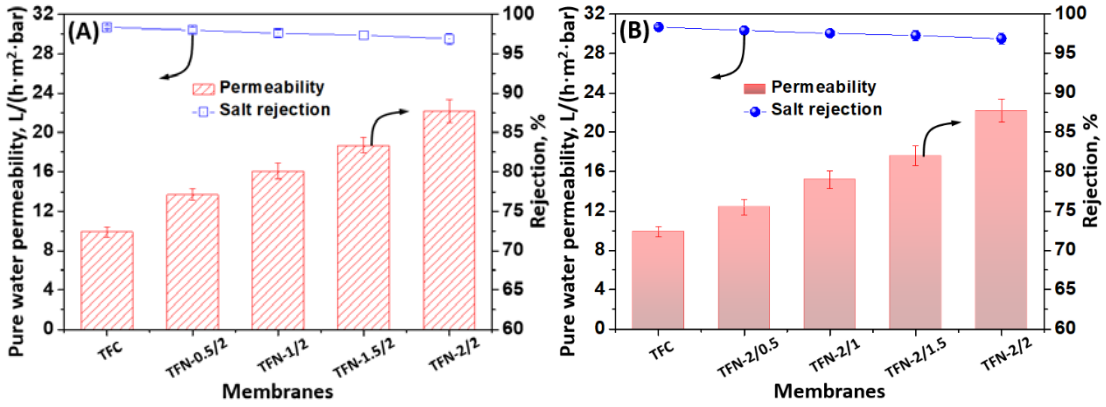

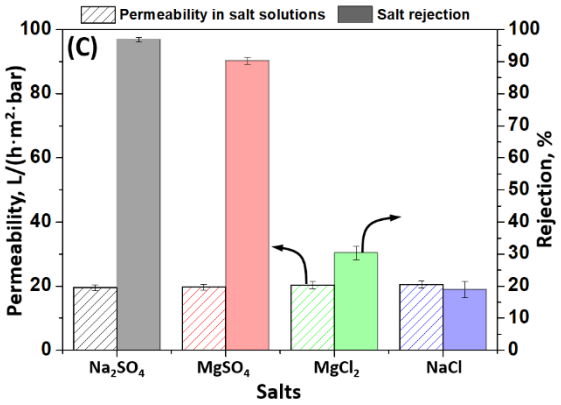

Fig. 9 Filtration performance of the fabricated TFN NF membrane with various (A) ageing times and (B) EPD times; (C) permeation flux and salt rejection of TFN-2/2 membrane in different salt solutions.

Aiming at enhancing the membrane performance, attempts have been made to control the growth of the ZIF-8 nanoparticles through manipulating the ageing time and EPD time. The ageing time and EPD time dominate the crystal structure of the ZIF-8 nanoparticles and their loading into the PA layer, which consequently affected the filtration performance (i.e., salt rejection and permeation flux) of the fabricated TFN membranes. The influence of the ageing time on the membrane performance was detected by varying the ageing time from 0.5 to 2 min while the EPD time was fixed at 2 min. As shown in **Fig. 9A**, the slight reduction in rejection of Na_2SO_4 for the fabricated TFN membranes was observed during the incorporation of the ZIF-8 nanoparticles into the PA layer. In particular, the extension of the ageing time could stimulate the growth of the ZIF-8 nanoparticles, allowing for an increasingly positive charge density on the ZIF-8 nanoparticles. Therefore, the incorporation of the ZIF-8 nanoparticles carrying positive charges into the PA layer would diminish the negative

charge density of the TFN membranes, which can also be confirmed by the reduction of negative charge on the PES (i.e., ZIF-8@PES) substrate deposited with the ZIF-8 nanoparticles (**Fig. 10**). This could reduce the electrostatic repulsion to the ions to some extent for enhanced salt permeation.

Simultaneously, extending the EPD duration can yield an increasing amount of the ZIF-8 nanoparticles incorporated into the PA layer of the TFN membranes, which also reduces the negative charges of the TFN membrane surfaces (**Fig. 10**) and thus promotes the salt permeation (**Fig. 9B**). On the other hand, the intercalation of the ZIF-8 interlayer into the PA layer results in a slight reduction in membrane pore size (slight reduction in MWCO of the TFN-2/2 membrane, Supplementary Fig. S1), which would reduce the size exclusion effect to the ions to some extent for salt permeation. However, an acceptably high Na_2SO_4 retention (above 96.9%) can be obtained for all the fabricated TFN membranes within an ageing time of 2 min and an EPD duration of 2 min.

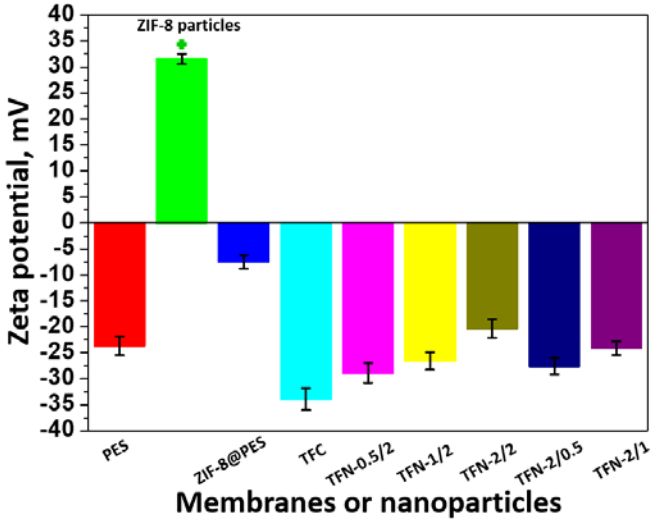

Fig. 10 Zeta potential of the TFN membrane after loading the ZIF-8 nanoparticles by EPD process.

On the other hand, the growth of the ZIF-8 nanoparticles with the ageing time and the increasing amount of the ZIF-8 nanoparticles deposited into the PA layer with the EPD duration would significantly enhance the permeation flux of the TFN membranes. Specifically, the permeation flux for the fabricated TFN membranes after the loading of ZIF-8 nanoparticles was remarkably elevated by a factor of 2.24, i.e., from 9.9±0.5 to 22.4±1.2 $L \cdot m^{-2} \cdot h^{-1} \cdot bar^{-1}$, within the ageing time of 2 min and EPD duration of 2 min (i.e., TFN-2/2). Generally, the enhancement in permeation flux of NF membrane is strongly related to the expansion of pore size and increase in surface hydrophilicity. However, in this case, the TFN membrane (i.e., TFN-2/2) has the nearly identical pore size and surface hydrophilicity with the TFC membrane, which can be demonstrated by the MWCO and water contact angle of these two membranes (**Supplementary Fig. S1** and **Table S1**). Therefore, such a significant enhancement in permeation flux of the TFN membrane (TFN-2/2) is mainly attributed to the fact that the loading of the ZIF-8 nanoparticles would create extra nano-channels and effective permeable area in the PA layer for enhanced water permeation.

In addition, the salt permeation properties of the TFN-2/2 NF membrane in the NaCl, $MgCl_2$ and $MgSO_4$ solutions were also investigated to reveal its desalination performance (**Fig. 9C**). As indicated in **Fig. 9C**, the TFN-2/2 membrane yielded a rejection of 90.3±1.1%, 30.4±2.0%, and 18.9±2.5% for $MgSO_4$, $MgCl_2$, and NaCl, respectively. The rejection order of different salts is Na_2SO_4 > $MgSO_4$ > $MgCl_2$ > NaCl for the TFN-2/2 NF membrane incorporated by the ZIF-8 nanoparticles. Such a salt rejection order is mainly due to the negatively-charged surface of the TFN-2/2

membrane which can effectively repulse the multivalent anion via Donnan effect [39]. On the other hand, the observed rejection of $MgCl_2$ was higher than that of NaCl for TFN-2/2 membrane, due to the fact that the hydrated radius of Mg^{2+} ion is larger than that of Na^+ ion, which can be effectively retained by the TFN membranes through enhanced size exclusion effect [40-42]. Specifically, the TFN-2/2 NF membrane shows a separation factor of 26.0 between Na_2SO_4 and NaCl, as reflected from the salt rejection order. This demonstrates a great potential of the TFN NF membrane incorporated with the ZIF-8 nanoparticles in separation of bivalent ions and monovalent ions. On the other hand, the permeation flux of the TFN membrane in all the salt (i.e., Na_2SO_4, $MgSO_4$, $MgCl_2$ and NaCl) solutions is slightly lower than that of the TFN membrane in the pure water. This is due to the osmotic pressure difference between feed side and permeate side of the TFN-2/2 membrane when filtrating the salt solutions. However, the permeation flux of the TFN-2/2 membrane (>19.5 $L \cdot m^{-2} \cdot h^{-1} \cdot bar^{-1}$) is still acceptably high for potential application.

Table 3 summaries the filtration performance of the state-of-the-art NF membranes reported in literature and the TFN NF membrane in this study. As indicated in Table 3, the deposition of the ZIF-8 nanoparticles by the EPD process could potentially endow the fabricated TFN NF membrane (i.e., TFN-2/2) with a superior permeability and an enhanced selectivity between monovalent and divalent salts, outperforming the state-of-the-art NF membranes reported in the literature and breaking through the tradeoff between permeability and solute selectivity.

437 **Table 3** Comparison of the state-of-the-art NF membranes reported in literature and

438 TFN nanofiltration membrane in this study

Membrane	Pressure (bar)	Salt rejection (%)				$S_{Na2SO4/NaCl}$	Pure water permeability ($L \cdot m^{-2} \cdot h^{-1} \cdot bar^{-1}$)	Ref.
		NaCl	Na_2SO_4	MgCl	$MgSO_4$			
NFM-4	6.0	34.0	97.6	-	92.7	27.5	13.2	[43]
$TFN_{PDA-SiNPs}$	6.0	35.0	97.0	68.0	94.0	21.7	13.3	[44]
GO-TFN	4.0	-	96.6	-	90.5	-	15.6	[45]
CS	6.0	32.2	90.8	-	73.7	7.4	5.7	[46]
TFN-PDP	6.0	44.1	98.1	43.1	97.9	28.0	9.9	[47]
PS/PES TFC	4.0	39.8	95.9	89.2	96.2	14.7	11.9	[48]
LBL	4.0	22.6	86.8	80.9	-	5.9	16.4	[41]
TFN-f0.02	8.0	47.1	95.8	90.0	97.7	12.6	4.9	[49]
TFNM with HZN_{CS}	-	38.2	94.7	-	93.4	11.7	10.5	[50]
TFN	6.0	20.0-30.0	98.0	-	90.0-98.0		14.6	[51]
ZIF-8 membrane	5.0	64.7	92.2	46.9	81.5	4.5	3.6	[52]
IISERP-COOH-COF1	2.0	82.9	97.2	90.6	99.6	6.1	0.5	[53]
TFN 0.3	5.0	77.6	96.6	-	95.0	6.6	2.4	[54]
ZIF-8/(TA-Zn^{2+})$_2$/PES	5.0	55.2	93.6	52.6	85.9	7.0	5.1	[55]
PA-flower (0.3 wt% MIL-101(Cr))	7.5	32.4	88.2	36.1	97.1	5.7	8.5	[56]
MSH@UiO-66-NH_2 TFN	15.0	36.4	82.9	-	94.4	3.7	5.3	[57]
UiO-66-NH_2@PA	10.0	22.0	97.4	-	91.0	30.0	9.4	[58]
TFN-300	4.0	29.0	95.0	65.0	94.0	14.2	8.5	[59]
TFN-4H	6.0	47.4	95.2	-	-	11.0	-	[60]
PDA/ZIF-8	6.0	16.4	83.4	-	-	5.0	4.8	[61]
TFN-2/2	4.0	18.9	96.9	30.4	90.3	26.2	22.4	This work

439

Moreover, the stability of the TFN membrane is of significance for its practical application. The long-term operation of the TFN-2/2 membrane in the Na_2SO_4 solution in a cross-flow mode was investigated (**Fig. 11**). As indicated in **Fig. 11A**, the TFN membrane yielded the almost constant permeation flux (permeation flux of 19.3~19.5 $L \cdot m^{-2} \cdot h^{-1} \cdot bar^{-1}$) and salt rejection ($Na_2SO_4$ rejection of 96.8~97.1%) in the Na_2SO_4 solution during a 36-h operation, indicating the long-term stability of the TFN membrane for potential in practical applications. As expected, the slight release of Zn^{2+} ion can be observed in the long-term operation (**Fig. 11B**). However, such a light release of Zn^{2+} ion has no pronounced impact on the membrane performance, since the interlayer of the ZIF-8 nanoparticles was well covered and intercalated into the PA layer of the TFN membranes, which can maintain the integrity of the PA layer. This result further demonstrates the superiority of the EPD process in intercalation of the ZIF-8 nanoparticles for fabrication of stable TFN membranes.

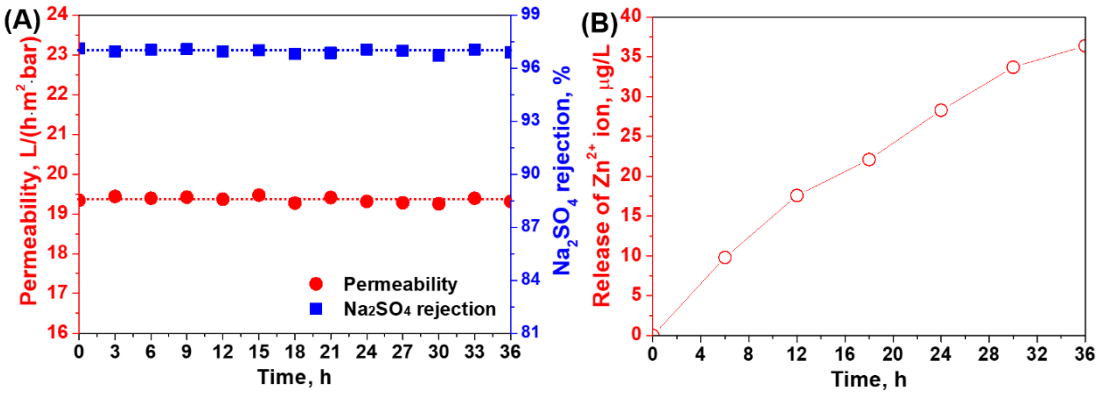

Fig. 11 (A) Long-time stability of the TFN-2/2 membrane; (B) release of Zn^{2+} ion from the TFN-2/2 membrane

4. Conclusions

In this study, a strategy of integration of the EPD process with vacuum filtration-assisted IP was proposed to design a high-performance ZIF-8 based TFN membrane. Through the EPD process, the ZIF-8 nanoparticles can be uniformly and sufficiently anchored into the PA layer to significantly tailor the surface structure and properties of the fabricated TFN nanofiltration membranes. At the condition of ageing time of 2 min and EPD duration of 2 min, the resultant TFN NF membrane (i.e., TFN-2/2) yielded an enhanced permeability of 22.4±1.2 $L \cdot m^{-2} \cdot h^{-1} \cdot bar^{-1}$, which was 2.24 folds higher than the pristine TFC NF membrane without loading of the ZIF-8 nanoparticles. Simultaneously, a considerably high rejection of 96.9±0.7% for Na_2SO_4 was obtained, breaking through the tradeoff between permeability and solute selectivity for the ZIF-8 incorporated TFN NF membrane. In addition, due to the less negative charge of the TFN NF membrane which was tailored by anchoring the ZIF-8 nanoparticles with positive charge, a very low rejection for NaCl was observed, which conferred the TFN nanofiltration membrane with a high selectivity between SO_4^{2-} and Cl^-. Based on these results, this study provides a useful guideline for precisely anchoring the nanomaterials into the PA layer to design the advanced NF membranes for target separations.

Acknowledgement

The authors would like to thank the funding support from the National Natural Science Foundation of China (Grant No.: 21908076).

References

[1] M.M. Mekonnen, A.Y. Hoekstra, Four billion people facing severe water scarcity,

480 Science Advances, 2 (2016) e1500323.
481 [2] J. Li, S. Yuan, J. Zhu, B. Van der Bruggen, High-flux, antibacterial composite
482 membranes via polydopamine-assisted PEI-TiO_2/Ag modification for dye removal,
483 Chemical Engineering Journal, 373 (2019) 275-284.
484 [3] X. Li, Y. Mo, W. Qing, S. Shao, C.Y. Tang, J. Li, Membrane-based technologies for
485 lithium recovery from water lithium resources: A review, Journal of Membrane Science,
486 591 (2019) 117317.
487 [4] X. Yang, L. Yan, J. Ma, Y. Bai, L. Shao, Bioadhesion-inspired surface engineering
488 constructing robust, hydrophilic membranes for highly-efficient wastewater
489 remediation, Journal of Membrane Science, 591 (2019) 117353.
490 [5] L.-Q. Li, Z.-M. Zhan, B.-Q. Huang, S.-M. Xue, C.-H. Ji, R.-Z. Wang, Y.-J. Tang,
491 Z.-L. Xu, RO membrane fabricated via a facile modified heat-treating strategy for high-
492 flux desalination, Journal of Membrane Science, 614 (2020) 118498.
493 [6] Z.-M. Zhan, Z.-L. Xu, K.-K. Zhu, S.-M. Xue, C.-H. Ji, B.-Q. Huang, C.Y. Tang, Y.-
494 J. Tang, Superior nanofiltration membranes with gradient cross-linked selective layer
495 fabricated via controlled hydrolysis, Journal of Membrane Science, 604 (2020) 118067.
496 [7] V. Freger, J. Gilron, S. Belfer, TFC polyamide membranes modified by grafting of
497 hydrophilic polymers: an FT-IR/AFM/TEM study, Journal of Membrane Science, 209
498 (2002) 283-292.
499 [8] S. Casanova, T.-Y. Liu, Y.-M.J. Chew, A. Livingston, D. Mattia, High flux thin-film
500 nanocomposites with embedded boron nitride nanotubes for nanofiltration, Journal of
501 Membrane Science, 597 (2020) 117749.

[9] P. Li, M. Zhang, Z. Zhai, M. Wang, P. Li, Y. Hou, Q. Jason Niu, Precise assembly of a zeolite imidazolate framework on polypropylene support for the fabrication of thin film nanocomposite reverse osmosis membrane, Journal of Membrane Science, 612 (2020) 118412.

[10] M. Safarpour, A. Khataee, V. Vatanpour, Thin film nanocomposite reverse osmosis membrane modified by reduced graphene oxide/TiO2 with improved desalination performance, Journal of Membrane Science, 489 (2015) 43-54.

[11] L. Jin, W. Shi, S. Yu, X. Yi, N. Sun, C. Ma, Y. Liu, Preparation and characterization of a novel PA-SiO2 nanofiltration membrane for raw water treatment, Desalination, 298 (2012) 34-41.

[12] J. Zhu, L. Qin, A. Uliana, J. Hou, J. Wang, Y. Zhang, X. Li, S. Yuan, J. Li, M. Tian, Elevated performance of thin film nanocomposite membranes enabled by modified hydrophilic MOFs for nanofiltration, ACS Applied Materials & Interfaces, 9 (2017) 1975-1986.

[13] M. Zhou, A. Vassallo, J. Wu, Toward the inverse design of MOF membranes for efficient D2/H2 separation by combination of physics-based and data-driven modeling, Journal of Membrane Science, 598 (2020) 117675.

[14] C.H. Hendon, D. Tiana, M. Fontecave, C.m. Sanchez, L. D'arras, C. Sassoye, L. Rozes, C. Mellot-Draznieks, A. Walsh, Engineering the optical response of the titanium-MIL-125 meta-organic framework through ligand functionalization, Journal of the American Chemical Society, 135 (2013) 10942-10945.

[15] X. Li, Y. Liu, J. Wang, J. Gascon, J. Li, B. Van der Bruggen, Metal–organic

524 frameworks based membranes for liquid separation, Chemical Society reviews, 46
525 (2017) 7124-7144.
526 [16] Y. Gong, S. Gao, Y. Tian, Y. Zhu, W. Fang, Z. Wang, J. Jin, Thin-film
527 nanocomposite nanofiltration membrane with an ultrathin polyamide/UIO-66-NH_2
528 active layer for high-performance desalination, Journal of Membrane Science, 600
529 (2020) 117874.
530 [17] E.L. Butler, C. Petit, A.G. Livingston, Poly(piperazine trimesamide) thin film
531 nanocomposite membrane formation based on MIL-101: Filler aggregation and
532 interfacial polymerization dynamics, Journal of Membrane Science, 596 (2020) 117482.
533 [18] M.-y. Zhang, X.-p. Wang, R. Lin, Y. Liu, F.-s. Chen, L.-s. Cui, X.-m. Meng, J. Hou,
534 Improving the hydrostability of ZIF-8 membrane by biomolecule towards enhanced
535 nanofiltration performance for dye removal, Journal of Membrane Science, 618 (2021)
536 118630.
537 [19] M. Navarro, J. Benito, L. Paseta, I. Gascon, J. Coronas, C. Tellez, Thin-film
538 nanocomposite membrane with the minimum amount of MOF by the Langmuir-
539 Schaefer technique for nanofiltration, ACS Applied Materials & Interfaces, 10 (2018)
540 1278-1287.
541 [20] C. Van Goethem, R. Verbeke, S. Hermans, R. Bernstein, I.F.J. Vankelecom,
542 Controlled positioning of MOFs in interfacially polymerized thin-film nanocomposites,
543 Journal of Materials Chemistry A, 4 (2016) 16368-16376.
544 [21] L. Wang, M. Fang, J. Liu, J. He, J. Li, J. Lei, Layer-by-Layer Fabrication of high-
545 performance polyamide/ZIF-8 nanocomposite membrane for nanofiltration

546 applications, ACS Applied Materials & Interfaces, 7 (2015) 24082-24093.
547 [22] J. Zhu, J. Hou, S. Yuan, Y. Zhao, Y. Li, R. Zhang, M. Tian, J. Li, J. Wang, B. Van
548 der Bruggen, MOF-positioned polyamide membranes with a fishnet-like structure for
549 elevated nanofiltration performance, Journal of Materials Chemistry A, 7 (2019) 16313-
550 16322.
551 [23] L. Besra, M. Liu, A review on fundamentals and applications of electrophoretic
552 deposition (EPD), Progress in Materials Science, 52 (2007) 1-61.
553 [24] S. Cabanas-Polo, A.R. Boccaccini, Electrophoretic deposition of nanoscale TiO_2:
554 technology and applications, Journal of the European Ceramic Society, 36 (2016) 265-
555 283.
556 [25] I. Hod, W. Bury, D.M. Karlin, P. Deria, C.W. Kung, M.J. Katz, M. So, B. Klahr, D.
557 Jin, Y.W. Chung, Directed growth of electroactive metal-organic framework thin films
558 using electrophoretic deposition, Advanced Materials, 26 (2014) 6295-6300.
559 [26] Z. Tan, S. Chen, X. Peng, L. Zhang, C. Gao, Polyamide membranes with nanoscale
560 Turing structures for water purification, Science, 360 (2018) 518-521.
561 [27] M.I. Baig, P.G. Ingole, J.-d. Jeon, S.U. Hong, W.K. Choi, H.K. Lee, Water vapor
562 transport properties of interfacially polymerized thin film nanocomposite membranes
563 modified with graphene oxide and GO-TiO_2 nanofillers, Chemical Engineering Journal,
564 373 (2019) 1190-1202.
565 [28] I.H. Aljundi, Desalination characteristics of TFN-RO membrane incorporated with
566 ZIF-8 nanoparticles, Desalination, 420 (2017) 12-20.
567 [29] J. Yin, E.-S. Kim, J. Yang, B. Deng, Fabrication of a novel thin-film nanocomposite

568 (TFN) membrane containing MCM-41 silica nanoparticles (NPs) for water purification,
569 Journal of Membrane Science, 423-424 (2012) 238-246.
570 [30] Y. Li, L.H. Wee, A. Volodin, J.A. Martens, I.F.J. Vankelecom, Polymer supported
571 ZIF-8 membranes prepared via an interfacial synthesis method, Chemical
572 Communication, 51 (2015) 918-920.
573 [31] D. Ragab, H.G. Gomaa, R. Sabouni, M. Salem, M. Ren, J. Zhu, Micropollutants
574 removal from water using microfiltration membrane modified with ZIF-8 metal organic
575 frameworks (MOFs), Chemical Engineering Journal, 300 (2016) 273-279.
576 [32] M. Son, H.-g. Choi, L. Liu, E. Celik, H. Park, H. Choi, Efficacy of carbon nanotube
577 positioning in the polyethersulfone support layer on the performance of thin-film
578 composite membrane for desalination, Chemical Engineering Journal, 266 (2015) 376-
579 384.
580 [33] J. Lin, C.Y. Tang, C. Huang, Y.P. Tang, W. Ye, J. Li, J. Shen, R. Van den Broeck, J.
581 Van Impe, A. Volodin, C. Van Haesendonck, A. Sotto, P. Luis, B. Van der Bruggen, A
582 comprehensive physico-chemical characterization of superhydrophilic loose
583 nanofiltration membranes, Journal of Membrane Science, 501 (2016) 1-14.
584 [34] S. Yu, S. Li, S. Huang, Z. Zeng, S. Cui, Y. Liu, Covalently bonded zeolitic
585 imidazolate frameworks and polymers with enhanced compatibility in thin film
586 nanocomposite membranes for gas separation, Journal of Membrane Science, 540
587 (2017) 155-164.
588 [35] S. Japip, S. Erifin, T.-S. Chung, Reduced thermal rearrangement temperature via
589 formation of zeolitic imidazolate framework (ZIF)-8-based nanocomposites for

590 hydrogen purification, Sep. Purif. Technol., 212 (2019) 965-973.
591 [36] F. Cacho-Bailo, B. Seoane, C. Téllez, J. Coronas, ZIF-8 continuous membrane on
592 porous polysulfone for hydrogen separation, Journal of Membrane Science, 464 (2014)
593 119-126.
594 [37] N. Jamil, N.H. Othman, N.H. Alias, M.Z. Shahruddin, R.A. Roslan, W.J. Lau, A.F.
595 Ismail, Mixed matrix membranes incorporated with reduced graphene oxide (rGO) and
596 zeolitic imidazole framework-8 (ZIF-8) nanofillers for gas separation, Journal
597 of Solid State Chemistry, 270 (2019) 419-427.
598 [38] D.W. Kim, K. Eum, H. Kim, D. Kim, M.D.d. Mello, K. Park, M. Tsapatsis,
599 Continuous ZIF-8/reduced graphene oxide nanocoating for ultrafast oil/water
600 separation, Chemical Engineering Journal, 372 (2019) 509-515.
601 [39] W. Ding, H. Zhuo, M. Bao, Y. Li, J. Lu, Fabrication of organic-inorganic
602 nanofiltration membrane using ordered stacking SiO_2 thin film as rejection layer
603 assisted with layer-by-layer method, Chemical Engineering Journal, 330 (2017) 337-
604 344.
605 [40] J. Li, Z. Zhao, S. Yuan, J. Zhu, B. Van der Bruggen, High-performance thin-film-
606 nanocomposite cation exchange membranes containing hydrophobic zeolitic
607 imidazolate framework for monovalent selectivity, Applied Sciences, 8 (2018) 759.
608 [41] T. Wang, J. Lu, L. Mao, Z. Wang, Electric field assisted layer-by-layer assembly
609 of graphene oxide containing nanofiltration membrane, Journal of Membrane Science,
610 515 (2016) 125-133.
611 [42] D. Hu, Z.-L. Xu, C. Chen, Polypiperazine-amide nanofiltration membrane

612 containing silica nanoparticles prepared by interfacial polymerization, Desalination,
613 301 (2012) 75-81.
614 [43] Z. Zhang, G. Kang, H. Yu, Y. Jin, Y. Cao, Fabrication of a highly permeable
615 composite nanofiltration membrane via interfacial polymerization by adding a novel
616 acyl chloride monomer with an anhydride group, Journal of Membrane Science, 570-
617 571 (2019) 403-409.
618 [44] M.B.M.Y. Ang, C.A. Trilles, M.R. De Guzman, J.M. Pereira, R.R. Aquino, S.-H.
619 Huang, C.-C. Hu, K.-R. Lee, J.-Y. Lai, Improved performance of thin-film
620 nanocomposite nanofiltration membranes as induced by embedded polydopamine-
621 coated silica nanoparticles, Separation and Purification Technology, 224 (2019) 113-
622 120.
623 [45] W. Zhao, H. Liu, N. Meng, M. Jian, H. Wang, X. Zhang, Graphene oxide
624 incorporated thin film nanocomposite membrane at low concentration monomers,
625 Journal of Membrane Science, 565 (2018) 380-389.
626 [46] Y.-J. Tang, L.-J. Wang, Z.-L. Xu, H.-Z. Zhang, Novel chitosan-piperazine
627 composite nanofiltration membranes for the desalination of brackish water and seawater,
628 Journal of Polymer Research, 25 (2018) 118.
629 [47] M.B.M.Y. Ang, Y.-L. Ji, S.-H. Huang, K.-R. Lee, J.-Y. Lai, A facile and versatile
630 strategy for fabricating thin-film nanocomposite membranes with polydopamine-
631 piperazine nanoparticles generated in situ, Journal of Membrane Science, 579 (2019)
632 79-89.
633 [48] X. Wei, X. Kong, C. Sun, J. Chen, Characterization and application of a thin-film

634 composite nanofiltration hollow fiber membrane for dye desalination and concentration,
635 Chemical Engineering Journal, 223 (2013) 172-182.
636 [49] G.S. Lai, W.J. Lau, P.S. Goh, A.F. Ismail, Y.H. Tan, C.Y. Chong, R. Krause-
637 Rehberg, S. Awad, Tailor-made thin film nanocomposite membrane incorporated with
638 graphene oxide using novel interfacial polymerization technique for enhanced water
639 separation, Chemical Engineering Journal, 344 (2018) 524-534.
640 [50] Z. Sun, Q. Wu, C. Ye, W. Wang, L. Zheng, F. Dong, Z. Yi, L. Xue, C. Gao, Nano-
641 void membranes embedded with hollow zwitterionic nanocapsules for superior
642 desalination performance, Nano letters, 19 (2019) 2953–2959.
643 [51] F. Xiao, X. Hu, Y. Chen, Y. Zhang, Porous Zr-Based metal-organic frameworks
644 (Zr-MOFs)-incorporated thin-film nanocomposite membrane toward enhanced
645 desalination performance, ACS Applied Materials & Interfaces, 11 (2019) 47390-
646 47403.
647 [52] Y. Xu, Y. Xiao, W. Zhang, H. Lin, L. Shen, R. Li, Y. Jiao, B.-Q. Liao, Plant
648 polyphenol intermediated metal-organic framework (MOF) membranes for efficient
649 desalination, Journal of Membrane Science, 618 (2021) 118726.
650 [53] C. Liu, Y. Jiang, A. Nalaparaju, J. Jiang, A. Huang, Post-synthesis of a covalent
651 organic framework nanofiltration membrane for highly efficient water treatment,
652 Journal of Materials Chemistry A, 7 (2019) 24205-24210.
653 [54] Y. Kang, M. Obaid, J. Jang, I.S. Kim, Sulfonated graphene oxide incorporated thin
654 film nanocomposite nanofiltration membrane to enhance permeation and antifouling
655 properties, Desalination, 470 (2019) 114125.

[55] Y. Xiao, W. Zhang, Y. Jiao, Y. Xu, H. Lin, Metal-phenolic network as precursor for fabrication of metal-organic framework (MOF) nanofiltration membrane for efficient desalination, Journal of Membrane Science, 624 (2021) 119101.

[56] N. Song, X. Xie, D. Chen, G. Li, H. Dong, L. Yu, L. Dong, Tailoring nanofiltration membrane with three-dimensional turing flower protuberances for water purification, Journal of Membrane Science, 621 (2021) 118985.

[57] M.B. Gohain, R.R. Pawar, S. Karki, A. Hazarika, S. Hazarika, P.G. Ingole, Development of thin film nanocomposite membrane incorporated with mesoporous synthetic hectorite and MSH@UiO-66-NH_2 nanoparticles for efficient targeted feeds separation, and antibacterial performance, Journal of Membrane Science, 609 (2020) 118212.

[58] Y. Lin, H.-C. Wu, Q. Shen, L. Zhang, K. Guan, T. Shintani, K.-L. Tung, T. Yoshioka, H. Matsuyama, Custom-tailoring metal-organic framework in thin-film nanocomposite nanofiltration membrane with enhanced internal polarity and amplified surface crosslinking for elevated separation property, Desalination, 493 (2020) 114649.

[59] S. Xiao, X. Huo, Y. Tong, C. Cheng, S. Yu, X. Tan, Improvement of thin-film nanocomposite (TFN) membrane performance by CAU-1 with low charge and small size, Separation and Purification Technology, (2021) 118467.

[60] Z. Liao, X. Fang, J. Xie, Q. Li, D. Wang, X. Sun, L. Wang, J. Li, Hydrophilic Hollow Nanocube-Functionalized Thin Film Nanocomposite Membrane with Enhanced Nanofiltration Performance, ACS Applied Materials & Interfaces, 11 (2019) 5344-5352.

678 [61] B. Zhao, X. Long, H. Wang, L. Wang, Y. Qian, H. Zhang, C. Yang, Z. Zhang, J. Li,
679 C. Ma, Y. Shi, Polyamide thin film nanocomposite membrane containing polydopamine
680 modified ZIF-8 for nanofiltration, Colloids and Surfaces A: Physicochemical and
681 Engineering Aspects, 612 (2021) 125971.
682